This article is made available via the ACS COVID-19 subset for unrestricted RESEARCH re-use and analyses in any form or by any means with acknowledgement of the original source. These permissions are granted for the duration of the World Health Organization (WHO) declaration of COVID-19 as a global pandemic.

ACS Biomaterials SCIENCE & ENGINEERING

pubs.acs.org/journal/abseba

Letter

Bioinspired Antimicrobial PLA with Nanocones on the Surface for Rapid Deactivation of Omicron SARS-CoV-2

Daniel J. da Silva, Adriana Duran, Aline D. Cabral, Fernando L. A. Fonseca, Shu Hui Wang, Duclerc F. Parra, Rodrigo F. Bueno, Inés Pereyra, and Derval S. Rosa*

Cite This: *ACS Biomater. Sci. Eng.* 2023, 9, 1891−1899

Read Online

ACCESS | Metrics & More | Article Recommendations | Supporting Information

ABSTRACT: Bioinspired bactericidal surfaces are artificial surfaces that mimic the nanotopography of insect wings and are capable of inhibiting microbial growth by a physicomechanical mechanism. The scientific community has considered them an alternative method to design polymers with surfaces that inhibit bacterial biofilm formation, suitable for self-disinfectant medical devices. In this contribution, poly(lactic acid) (PLA) with nanocone patterns was successfully produced by a novel two-step procedure involving copper plasma deposition followed by argon plasma etching. According to reverse transcription-quantitative polymerase chain reaction tests, the bioinspired PLA nanostructures display antiviral performance to inactivate infectious Omicron severe acute respiratory syndrome coronavirus 2 particles, reducing the amount of the viral genome to less than 4% in just 15 min due to a possible combined effect of mechanical and oxidative stress. The bioinspired antiviral PLA can be suitable for designing personal protection equipment to prevent the transmission of contagious viral diseases, such as Coronavirus Disease 2019.

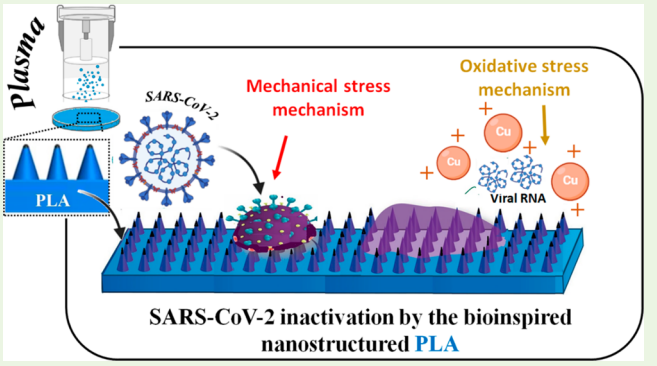

KEYWORDS: *SARS-CoV-2, surface, nanotopography, copper, poly(lactic acid)*

1. INTRODUCTION

The global pandemic of Coronavirus Disease 2019 (COVID-19) caused by Severe Acute Respiratory Syndrome Coronavirus 2 (SARS-CoV-2) has evidenced to human beings that there is a need to develop smart materials with viricidal properties to ensure the protection of people to direct contact with surfaces or air contaminated by viruses in open or closed spaces. It should be pointed out that the SARS-CoV-2 virus maintains its transmission and infection potential for 2 and 3 days on the surface of polypropylene and stainless steel, respectively.[1] Furthermore, people spend about 90% of their time indoors (hospitals, schools, and universities, among others), where airborne diseases' transmission is a critical epidemiological issue. Among the materials available and used for the manufacture of personal protective equipment (PPE), poly(lactic acid) (PLA) has been widely used in medical implants in the form of screws, pins, rods, and orthopedic devices.[2] In addition, PLA is biodegradable and can be produced from natural raw materials such as rice, corn starch, potatoes, and other renewable resources, which are characteristics considered important to minimize environmental impacts caused by the discarding of plastic residues.[3,4] This polymer can be processed by three-dimensional (3D) printing technologies, including the FDM (Fused Deposition Modeling), aiming for implants and other devices for healthcare purposes, including PPE.

Mother nature shows that surfaces structured with micro- and nanopatterns can inhibit biofilm formation, killing bacteria through mechanical stress. The nanostructured surfaces observed in wings from cicada, damselfly, dragonfly, shark skin, and the lotus leaf show patterns with such bactericidal activity, having attracted the attention of several studies.[5,6] In addition to the ability to confer bactericidal properties, these surfaces can present superhydrophobicity, being suitable for different technological applications, such as the design of self-cleaning smart textiles.[7,8] In general, bioinspired nanostructured surfaces are obtained by plasma technologies.[9,10] However, it is not a simple task to achieve a surface topography similar to natural surfaces that exhibit antibacterial properties with nanopillar (conical shape) dimensions observed on the wing of the *Mogannia hebes* (height of 164 nm, diameter of 85 nm, spacing of 95 nm).[11]

Received: December 21, 2022
Accepted: January 25, 2023
Published: March 7, 2023

Downloaded via UNIV OF SAO PAULO on April 12, 2023 at 11:02:24 (UTC).
See https://pubs.acs.org/sharingguidelines for options on how to legitimately share published articles.

© 2023 American Chemical Society

https://doi.org/10.1021/acsbiomaterials.2c01529
ACS Biomater. Sci. Eng. 2023, 9, 1891−1899

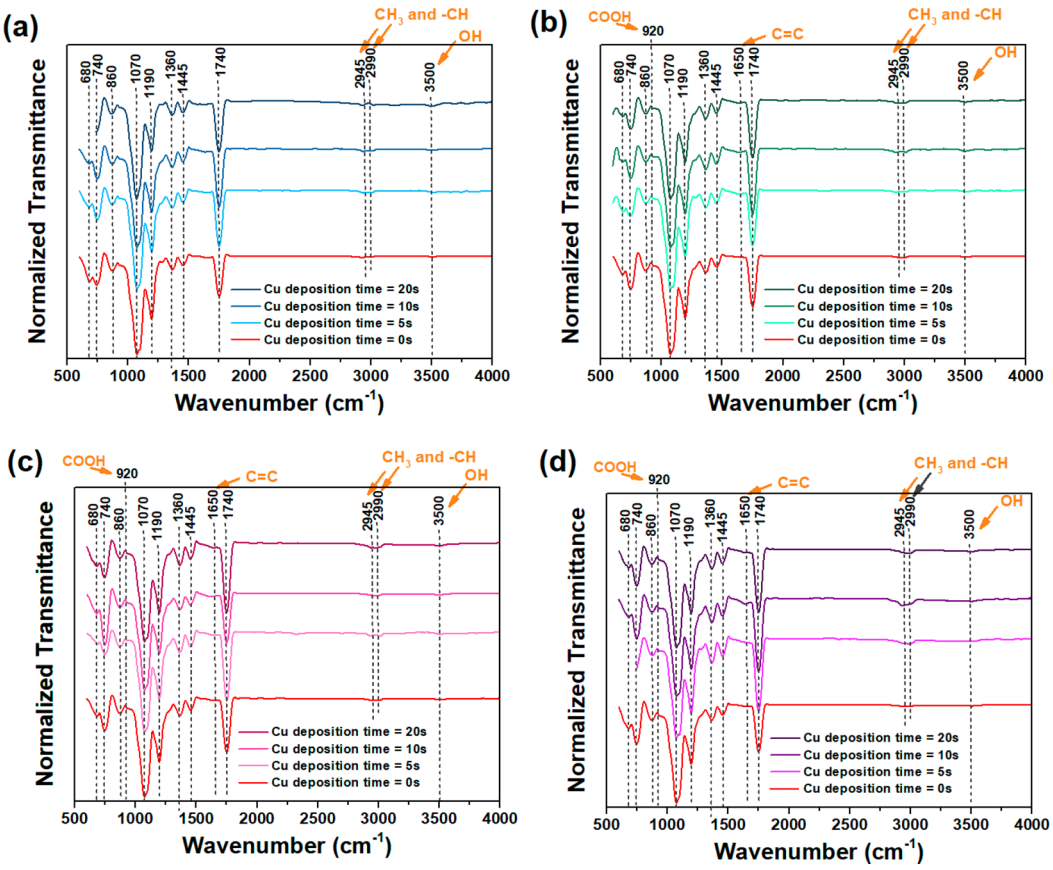

Figure 1. FTIR spectra of the copper-coated PLA samples using different deposition times (5, 10, and 20 s) and plasma etching times: 0 (a), 30 (b), 60 (c), and 120 s (d). Plasma etching was performed after metallic deposition. *Plasma etching time of 0 s means the sample was not plasma etched after the copper coating.

Table 1. Effect of Process Parameters (Copper Deposition Time and Plasma Etching) on the Relative Intensity (H_R) of FTIR Signals Associated with PLA Degradation[a]

Parameter	Functional group (important positive effects on H_R)	Functional group (important negative effects on H_R)	Functional group (minor effects on H_R)
Copper deposition time	CH + CH_3 (2990 cm^{-1})	COOH (920 cm^{-1})	All (except COOH and CH + CH_3, 2990 cm^{-1})
Plasma *etching* time	CH + CH_3 (2990 cm^{-1})		All (except CH + CH_3, 2990 cm^{-1})
Simultaneous interaction of parameters			All

[a]Results from t-tests and Bonferroni tests presented in Pareto charts. Negative Effects: H_R reduction. Positive effects: H_R increase. H_R was calculated for the functional groups: C═O (1750 cm^{-1}), COOH (920 cm^{-1}), C−O (secondary alcohol and PLA hydrolysis, 1260 cm^{-1}), C═C (1650 cm^{-1}), CH + CH_3 (2945 cm^{-1}), CH + CH_3 (2990 cm^{-1}), and OH (3600 cm^{-1}).

Since SARS-CoV-2 particles have diameters of 150−200 nm,[12] obtaining surfaces with nanocones with such dimensions would be interesting to assess whether this virus is susceptible to mechanical stress from bacteria. To the best of our knowledge, there are no studies about the virucidal activity of bioinspired surfaces. Then, in this contribution, we develop a new method to obtain PLA with a surface containing nanopatterns with conical shape, using copper deposition by plasma sputtering to obtain "copper nanomasks" and argon plasma etching as a surface nanostructuring agent. Such a surface was successfully designed by adjusting the process parameters of copper magnetron sputtering deposition and plasma etching, and it presented the potential to quickly destroy or deactivate the SARS-CoV-2 virus through the combined antiviral action of nanostructured topography (a physicomechanical mechanism) and copper (an oxidative mechanism), which is a metal with intrinsic antimicrobial activity via release of metal ion and generation of reactive oxygen species (ROS).[13]

2. RESULTS AND DISCUSSION

As shown in Figure 1 and detailed in Table 2S, PLA displays characteristic infrared absorption bands due to bond deformations at 1070 cm^{-1} (COC symmetric (sym.) stretching), 1190 cm^{-1} (asymmetric stretching of COC), 1360 cm^{-1} (CH deformation, CH_3 sym. bending), 1445 cm^{-1} (CH_3 bending), and 1740 cm^{-1} (C═O stretching).[14−19] Other minor absorptions due to CC stretching are attributed to polymer morphology deformations. The maximum intensity bands at 740 and 950 cm^{-1} can be assigned to the crystalline phase, while those at 860 and 920 cm^{-1} are from the amorphous phase.[20,21] Thus, changes in those peaks are often

https://doi.org/10.1021/acsbiomaterials.2c01529
ACS Biomater. Sci. Eng. 2023, 9, 1891−1899

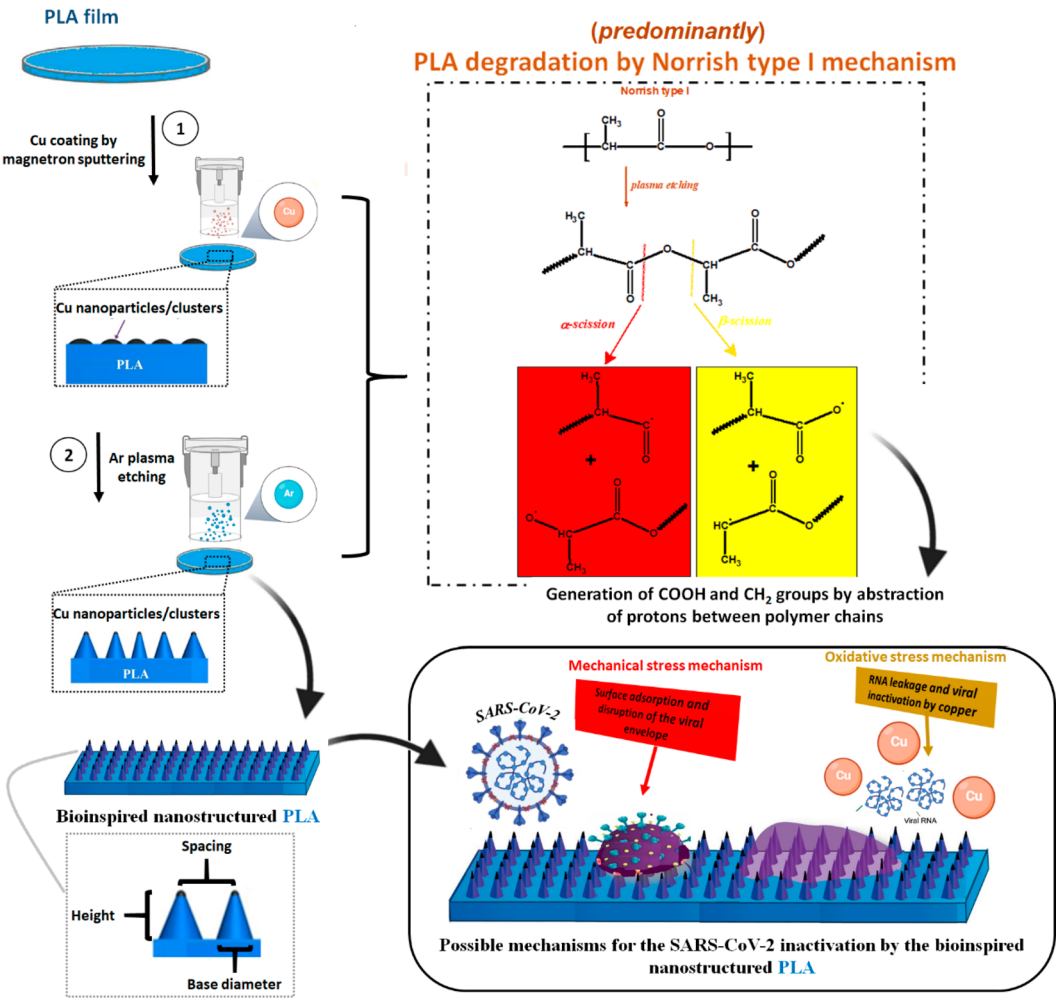

Figure 2. Schematic illustration of the PLA film coating with copper, chemical reactions associated with PLA degradation by Norrish type I mechanism during copper deposition, and Ar plasma etching. Also, the possible inactivation mechanisms of the SARS-CoV-2 virions are illustrated.

attributed to induced secondary crystallization. Inevitably, plasma treatment leads to polymer degradation. PLA is expected to undergo random chain scission under plasma; hence, besides cross-linking and degradation, induced oxidation processes may take place in the presence of dissolved water and O_2 molecules, leading to products containing hydroxyl ($\nu_{OH} \approx 3350$ cm^{-1}; $\delta_{OH} \approx 1350$ cm^{-1}; $\delta_{OH} \approx 650$ cm^{-1}), carboxylic acid ($\nu_{C=O} \approx 1700$ cm^{-1}, $\nu_{COOH} \approx 3500-3000$ cm^{-1}), anhydride ($\nu \approx 1780$ cm^{-1}), and vinyl ($\nu_{CH} \approx 3010$ cm^{-1}; $\nu_{CC} \approx 1650$ cm^{-1}; $\delta_{CH} \approx 990$ cm^{-1}/ ~910 cm^{-1}; ~690 cm^{-1}) moieties.[22] To analyze the PLA degradation after copper deposition and surface plasma etching, the relative intensity (H_R) for several infrared transmittance signals associated with the PLA degradation was calculated: C=O (1750 cm^{-1}), COOH (920 cm^{-1}), C−OH (secondary alcohol, 1260 cm^{-1}), C=C (1650 cm^{-1}), CH + CH_3 (2945 cm^{-1}), and CH + CH_3 (2990 cm^{-1}). Also, H_R response curves and their respective Pareto charts were determined using metal deposition and plasma etching times as process variables (Figures 1S and 2S). The Pareto charts are suitable for identifying the effects of surface plasma modification time on H_R, using an experimental design with factorial analysis. Table 1 details a summary of the effects of metal deposition time and plasma etching on the relative intensity (H_R) of Fourier transform infrared (FTIR) signals related to PLA degradation. The combination of analysis of variance (ANOVA) and factorial analysis with t test and Bonferroni test enables us to statistically evaluate the effects of different factors (isolated and combined) on a property/signal of interest, such as the H_R values. Prolonging the copper deposition process increases the H_R for CH + CH_3 (2990 cm^{-1}) but reduces that of COOH (920 cm^{-1}) probably due to amorphous(920)-crystalline(950) interconversion occasioned by plasma local heating effects. Plasma etching exposure time of copper-coated PLA films positively affects (i.e., increases) the H_R for the FTIR signal at 2990 cm^{-1}.

The ANOVA results for H_R do not indicate significant effects of the copper deposition and plasma etching times on the C−OH signal of secondary alcohols (1260 cm^{-1}), probably because the secondary alcohols tend to recombine and form molecules with C=C bonds in degraded PLA.[17] Therefore, the relative intensity signal of C−O (1260 cm^{-1}) is unchanged even though this C−O signal is strong and wide for many organic compounds with this bond extending over a wide range, but that for the C=C signal (1650 cm^{-1}) increases instead. The O−H bending at 1350 cm^{-1} also is subjected to interference from the C−H bending signal, influencing the degradation evaluation of the PLA samples by FTIR spectroscopy.

https://doi.org/10.1021/acsbiomaterials.2c01529
ACS Biomater. Sci. Eng. 2023, 9, 1891−1899

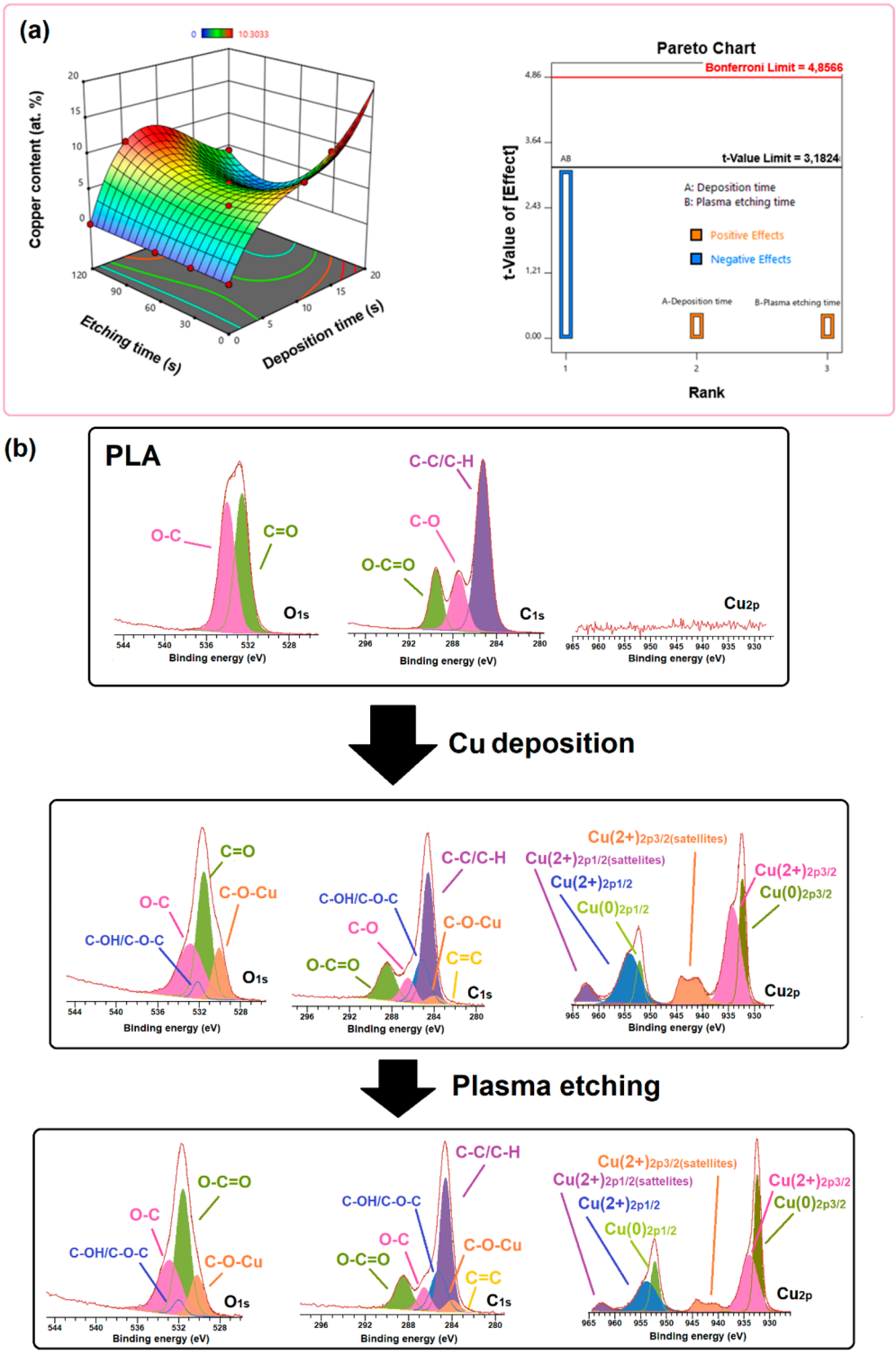

Figure 3. (a) Copper atomic concentration in copper-coated PLA samples from the XPS data: response surface (left image) and Pareto chart (right image) from the factorial analysis for the effect of factors (metal deposition time and plasma etching time), using ANOVA. AB: simultaneous interaction of factors A and B. Negative effect: reduces the property. Positive effect: increases the property. (b) O_{1s}, C_{1s}, and Cu_{2p} regions of XPS high-resolution spectra from the PLA before and after Cu deposition and plasma etching. 3D response surface fitting parameters are detailed in Supporting Information.

The increase in C═C and COOH abundance is connected with the products from PLA degradation via the Norrish type II mechanism due to ester bond-breaking under scission of the PLA polymer chains via cis-elimination reactions selectively triggered by the transition of electrons in the carbonyl without the production of free radicals.[23−25] According to the statistical results on H_R, copper leads to PLA degradation predominantly by the Norrish type I mechanism in which, after carbonyl excitation, an α-carbonyl bond undergoes homolytic cleavage, followed by hydrogen abstraction by formed free radicals (O═

https://doi.org/10.1021/acsbiomaterials.2c01529
ACS Biomater. Sci. Eng. 2023, 9, 1891−1899

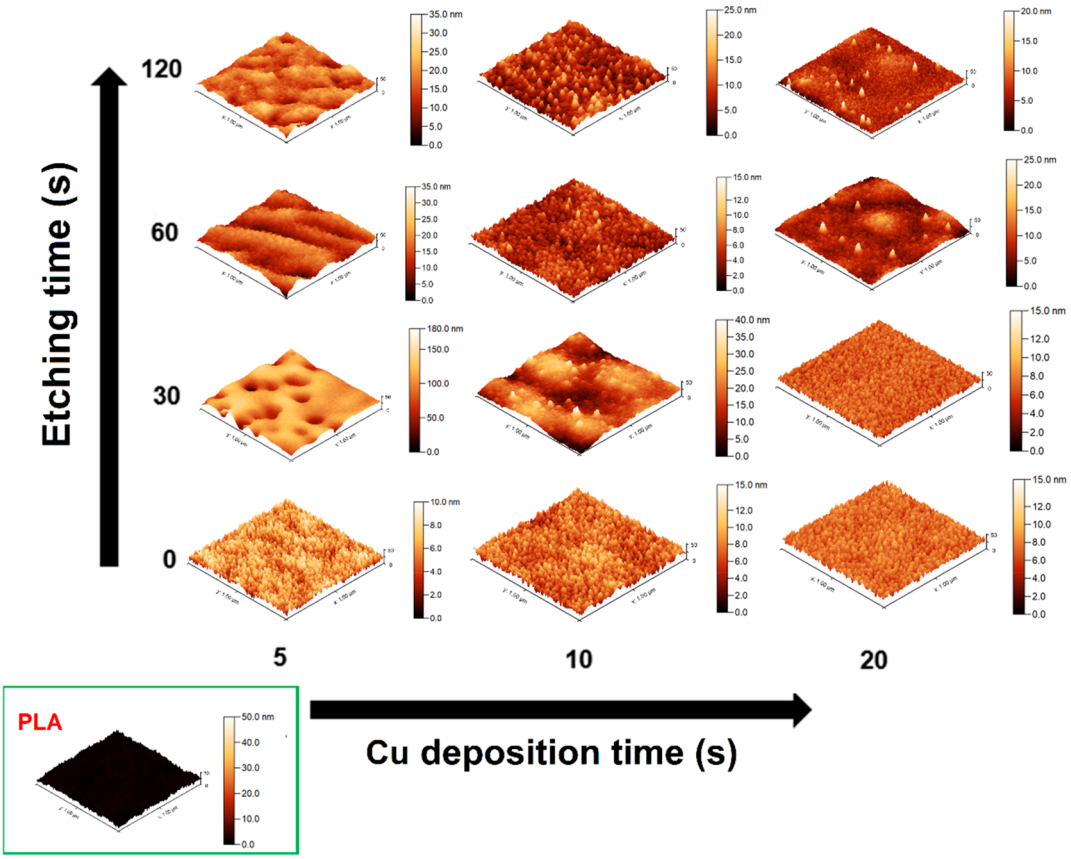

Figure 4. AFM images of the copper-coated PLA samples using different deposition times (5, 10, and 20 s) and plasma etching times (0, 30, 60, and 120 s). Plasma etching was performed after metallic deposition. Scan area = 1 μm × 1 μm. Size bars present different scales for each AFM image. *Plasma etching time of 0 s means the sample was not plasma-etched after the copper coating.

C•, O═C−O•, C−O•, and CH•) (Figure 2) that can continue the degradation of PLA[23,24] and can cause both cross-linking and random scission of PLA polymeric chains.[25] In addition, the secondary reactions can increase the amount of carboxylic acid, aldehyde, vinyl, and methyl groups on the PLA surface. In the case of Cu-coated PLA, the COO• radicals are unlikely to convert to COOH, due to copper availability, forming carboxylate instead, which explains the minor effect of the plasma process parameters on the H_R of the OH groups (3600 cm^{-1}) shown in the Pareto charts.

The copper atomic content on the PLA surface from X-ray photoelectron spectroscopy (XPS) measurements (Figure 3S) is slightly improved by the metal deposition time. However, there is a minor combined simultaneous effect of the plasma etching time and metal deposition time, as indicated by the t-values in the Pareto chart in Figure 3a. PLA shows characteristic binding energies associated with the O−C (287 eV in the C_{1s} region, 534 eV in the O_{1s} region), C═O (289.8 eV in the C_{1s} region, 531.5 eV in the O_{1s} region), and C−C/C−H 312 (285.1 eV in the C_{1s} region) chemical bonds (Figure 3b).[26−29]

The XPS spectra confirm the PLA degradation products indicated by FTIR data, presenting XPS signals associated with C−OH/C−O−C bonds (285.4 eV in the C_{1s} region, 533.5 eV in the O_{1s} region) and C═C bonds (282.8 eV in the C_{1s} region).[30] The copper film is chemically linked on the surface of the PLA substrate by C−O−Cu bonds (284.1 eV in the C_{1s} region, 531.5 eV in the O_{1s} region) since all copper-coated PLA present Cu^{2+} ions at the surface due to the binding signals at 963.5 eV (Cu^{2+} $2p_{1/2}$ satellites), 954.6 eV (Cu^{2+} $2p_{1/2}$), 944.1 eV (Cu^{2+} $2p_{3/2}$ satellites), 941.2 eV (Cu^{2+} $2p_{3/2}$ satellites), and 933.9 eV (Cu^{2+} $2p_{1/2}$) on Cu_{2p} XPS spectra.[31−33] Even after plasma etching, all copper-coated PLA display metallic copper (Cu^0) at the surface, confirmed by the XPS characteristic signals at 933 (Cu^0 $2p_{3/2}$) and 952.5 (Cu^0 $2p_{1/2}$).

The average transparency of the pristine PLA film is 59 ± 11%, but it is reduced with the Cu coating, mainly after the plasma etching treatment, as shown in the Pareto charts in Figures 4S and 5S. The accentuation of the PLA degradation, due to the plasma etching, reduced the PLA transparency and caused yellowing. The light yellow coloration of PLA became more evident after sputtering deposition of copper for 120 s (Figure 6S).

The atomic force microscopy (AFM) topographic images of the copper-coated PLA films are shown in Figure 4. There are significant topographical changes of the PLA substrate due to the Cu deposition time and plasma etching time, leading to the formation of nanocones on the PLA surface of several samples that depends on the parameters of the plasma treatment(s). In their review, Phan et al.[34] describe the mechanisms in plasma technologies responsible for the nanostructures on polymeric substrates, which involve pattern formation due to the preferential etching of polymers since the metal clusters work as an etching mask ("hard" plasma inhibitors) on polymeric surfaces, as illustrated in Figure 2.

According to AFM images (Figure 4), the PLA substrates present nanocones on their surface after 5 s of copper

https://doi.org/10.1021/acsbiomaterials.2c01529
ACS Biomater. Sci. Eng. 2023, 9, 1891−1899

deposition, but the plasma etching causes the destruction of these nanostructures on the PLA surface. However, the plasma etching does not remove the nanocones of the PLA substrate if the copper plasma deposition extends for 10 and 20 s, though the aspect ratio (feature height/base diameter) and spacing of the nanocones change (Figure 7S). While the aspect ratio is significantly increased by the plasma etching time, the diameter and spacing are improved by the metal deposition time. The root-mean-square roughness (R_q) calculated over the total area of the PLA samples suffers minor effects on the plasma etching and copper plasma deposition times evaluated in this work, as indicated by the Pareto chart in Figure 7S.

The dispersive (γ_s^{LW}) and polar (γ_s^{p}) components of the total surface free energy (γ_s^{total}) were calculated with the contact angles measured per sessile drop and using the Cassie-Bexter and Wenzel factors to consider the topography effects on total surface free energy (γ_s^{total}) of the copper-coated PLA samples. According to the design of experiments (Figure 8S), these surface parameters are not significantly changed by the plasma etching and metal plasma deposition times. γ_s^{p} and γ_s^{total} of the PLA samples tend to reduce due to the increase in the duration of the plasma etching and metal deposition, but the prolongation of the plasma etching slightly increases γ_s^{LW}. The pristine PLA presents γ_s^{total} of 164 ± 5 mJ/m^2, which is a value superior to surface energy data reported in the literature for PLA (typically from 40 to 110 mJ/m^2).[18,35] Commonly, these γ_s^{LW} data are determined without considering the surface defects (cracks, cavities, and voids) on the PLA substrates. Popelka et al.[36] observed the reduction of γ_s^{LW} and γ_s^{total} for PLA after plasma etching. Izdebska-Podsiadły et al.[37] observed the increase of the surface free energy of PLA after Argon plasma etching, but to the best of our knowledge, there are no studies about the γ_s^{total} changes of Cu-coated PLA substrates to compare our results.

The alterations of the γ_s^{LW}, γ_s^{p}, and γ_s^{total} are connected to the PLA degradation products and copper content fixation during the plasma treatments, which changes the amount of C═C, COOH, CH_2, and COO-Cu groups at the PLA surface. According to C_{1s} XPS data (Figure 3), the XPS signal area of the CH_2 and C═C bonds increases while the signal area of the C−O bonds reduces at the PLA surface due to the plasma treatments, justifying the increase of the γ_s^{LW}.

All Cu-coated PLA samples reduce the amplified RNA genetic material of the Omicron SARS-CoV-2 with just 15 min of direct contact with the viral inoculum, according to the quantitative reverse transcription-polymerase chain reaction (RT-qPCR) assays shown in Figure 5a. The Omicron strain is an SARS-CoV-2 variant that presents several mutations in RNA segments associated with the synthesis of viral proteins, such as Spike (S), Envelope (E), Membrane (M), and Nucleocapsid (N). Besides the high infectivity, the Omicron strain presents N mutations connected with new alternative mechanisms of the virus to evade the host immune response.[38] The Pareto charts from the RT-qPCR data (Figure 5b) suggest that the plasma etching times applied to design the bioinspired nanostructured surfaces on PLA slightly reduced the amplified RNA number, even though the plasma etching tends to reduce the copper content onto the PLA surface.

The reduction in the number of amplified RNA copies by RT-qPCR involves the viral capsid disruption (constituted by biological molecules, such as proteins and lipids) followed by RNA irreversible damages.[39−43] All Cu-coated samples display high antiviral capacity, reducing the amplified RNA copies by

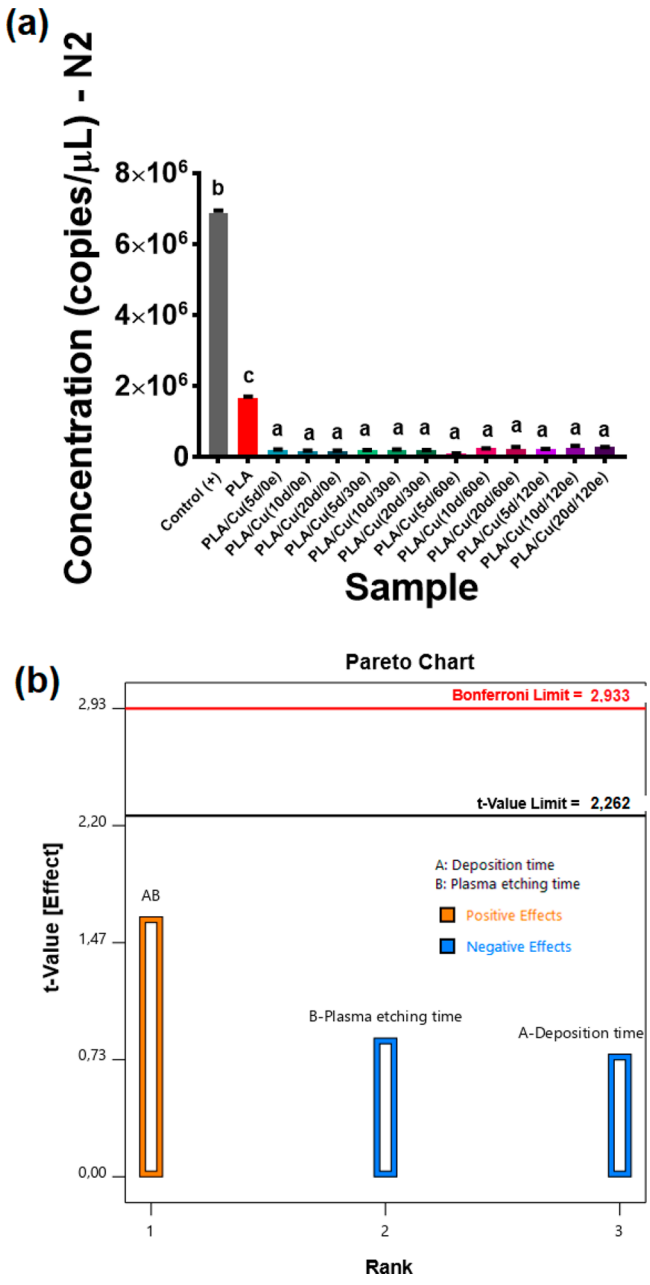

Figure 5. (a) Amplified RNA by RT-qPCR for Omicron SARS-CoV-2 using the N2 gene targets after 15 min of exposure with the PLA samples. Graph bars with different letters (a, b, and c) are significantly different, according to Tukey's test using a 95% reliability level. Cycle threshold (Ct) values were lower than 30. (b) Pareto charts (right) from the factorial analysis for the effect of factors (metal deposition time and plasma etching time) over the RT-qPCR data, using ANOVA. AB: simultaneous interaction of factors A and B. Factors above the Bonferroni threshold almost certainly have major effects on the property. Factors above the t-value threshold have potentially major effects on the property. Factors below the t-value threshold have minor effects on the property. Negative effect: reduces the property. Positive effect: increases the property. The samples were named PLA/Cu(*Y*d-*T*e), where *Y* is the copper deposition time by magnetron sputtering (5, 10, and 20 s), and *T* is the time used in the plasma etching treatment (0, 30, 60, and 120 s). *Plasma etching time of 0 s means the sample was not plasma-etched after the copper coating.

https://doi.org/10.1021/acsbiomaterials.2c01529
ACS Biomater. Sci. Eng. 2023, 9, 1891−1899

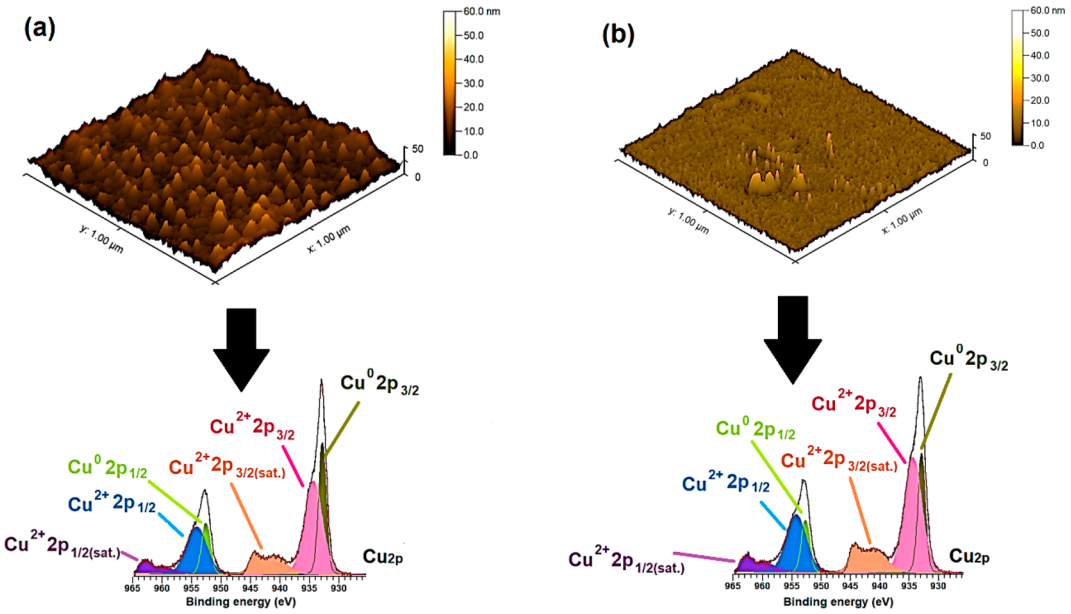

Figure 6. AFM image and XPS spectra (Cu_{2p} region) from a copper-coated PLA (a) before and (b) after wear.

more than 90% with respect to the results from the PLA sample, which does not present intrinsic antiviral properties. In a recent work, Meister et al.[44] reported that silicone substrates coated with copper could inhibit SARS-CoV-2 virions when the Cu ion release is higher than 50 μg/mL, which is a minimum antiviral dose higher than that observed for silver.

To elucidate if the nanocone patterns contribute to the virions' deactivation by mechanical stress, we removed the nanopatterns on a Cu-coated PLA sample by 20 wear cycles. The AFM image and the XPS spectra of this sample in Figure 6 prove the absence of nanopatterns on the Cu-coated surface after wear. At the same time, the reduction fold for the amplified RNA copies reduction remained at 70% concerning the results from the uncoated PLA sample, which suggests a poor contribution of the mechanical stress from the biomimetic topography to the final antimicrobial activity of the Cu-coated PLA. Then, the deactivation of virions is due to the copper ion release and ROS generation. The slight diminishment of fold reduction in the amplified RNA copies is due to the slight reduction of the copper content at the Cu-coated PLA surface caused by the wear.

3. CONCLUSIONS

We assembled PLA with a bioinspired surface containing conical nanostructures by combining copper plasma deposition and plasma etching, a new approach using low plasma treatment times. PLA has no intrinsic antiviral features, but the Cu-coated nanostructured PLA reduces the amplified RNA; RT-qPCR is reduced from 6.88 ± 0.05 Mcopies/μL (control) to lower than 0.26 ± 0.01 Mcopies/μL after just 15 min of direct contact with an Omicron SARS-CoV-2 inoculum from patients infected with COVID-19. The plasma treatment causes the PLA degradation via Norrish mechanisms, predominantly Norrish type I, according to FTIR and XPS data combined with the factorial analyses using the design of experiments.

The copper plasma deposition and plasma etching times change the aspect ratio (feature height/base diameter) and spacing of the nanocones, also affecting the total surface free energy (γ_s^{total}) and its dispersive (γ_s^{LW}) and polar (γ_s^{p}) components. Our results suggest that the nanocone patterns do not contribute to the antiviral properties of the Cu-coated PLA by a mechanical stress mechanism.

4. MATERIALS AND METHODS

The materials used and the experimental methods are detailed in the Supporting Information (available on the Internet).

■ ASSOCIATED CONTENT

Data Availability Statement

The data supporting this study's findings are available from the corresponding author upon reasonable request.

Supporting Information

The Supporting Information is available free of charge at https://pubs.acs.org/doi/10.1021/acsbiomaterials.2c01529.

Infrared absorption signals characteristic of PLA (Table 2S); Relative intensity (H_R) of FTIR absorption signals (Cu-coated PLA samples) (Figures 1S and 2S); 3D polynomial curve-fitting data for the H_R surface responses obtained from the experiment design of the FTIR data (Table 3S); XPS spectra of Cu-coated PLA samples using different deposition and plasma etching times (Figure 3S); 3D polynomial curve-fitting data for the surface response obtained by the experiment design (Table 4S); UV−vis transmittance spectra of copper-coated PLA using different deposition and plasma etching times (Figure 4S); Average transmittance of the Cu-coated PLA films (Figure 5S); Image of PLA films coated with copper using different metal deposition and plasma etching times (Figure 6S); 3D curve fitting data using polynomial models for average transparency from Cu-coated PLA samples (Table 5S); R_q and Pareto charts from AFM data of the Cu-coated PLA films (Figure 7S); 3D polynomial curve-fitting data for the surface response obtained by the experiment design of the R_q (Table 6S); γ_s^{LW}, γ_s^{p}, and γ_s^{total} from the Cu-coated PLA films (Figure 8S); 3D polynomial curve-fitting data

https://doi.org/10.1021/acsbiomaterials.2c01529
ACS Biomater. Sci. Eng. 2023, 9, 1891−1899

for the surface response obtained by the experiment design of γ_s^{LW}, γ_s^{p}, and γ_s^{total} (Table 7S) (PDF)

Accession Codes

Not applicable.

AUTHOR INFORMATION

Corresponding Author

Derval S. Rosa − *Center for Engineering, Modeling, and Applied Social Sciences, Federal University of ABC, 5001 Bangú, Santo André, SP, Brazil;* orcid.org/0000-0001-9470-0638; Email: dervalrosa@yahoo.com.br

Authors

Daniel J. da Silva − *Center for Engineering, Modeling, and Applied Social Sciences, Federal University of ABC, 5001 Bangú, Santo André, SP, Brazil; Department of Metallurgical and Materials Engineering, Polytechnic School, University of São Paulo, 05508-030 São Paulo, SP, Brazil;* orcid.org/0000-0002-1529-4895

Adriana Duran − *Center for Engineering, Modeling, and Applied Social Sciences, Federal University of ABC, 5001 Bangú, Santo André, SP, Brazil*

Aline D. Cabral − *Center for Engineering, Modeling, and Applied Social Sciences, Federal University of ABC, 5001 Bangú, Santo André, SP, Brazil*

Fernando L. A. Fonseca − *Department of Clinical Analysis, Faculty of Medicine of ABC, 2000 Santo André, SP, Brazil*

Shu Hui Wang − *Department of Metallurgical and Materials Engineering, Polytechnic School, University of São Paulo, 05508-030 São Paulo, SP, Brazil*

Duclerc F. Parra − *Nuclear and Energy Research Institute, National Nuclear Energy Commission/SP, 2242 São Paulo, SP, Brazil;* orcid.org/0000-0002-6481-0155

Rodrigo F. Bueno − *Coordinator of the COVID-19 Monitoring Network in Wastewater National Water and Basic Sanitation Agency, Ministry of Science, Technology and Innovation and Ministry of Health, Brazil. Center for Engineering, Modeling, and Applied Social Sciences, Federal University of ABC, 5001 Bangú, Santo André, SP, Brazil*

Inés Pereyra − *Department of Electronic Systems Engineering, Polytechnic School, University of São Paulo, 2643 São Paulo, SP, Brazil*

Complete contact information is available at: https://pubs.acs.org/10.1021/acsbiomaterials.2c01529

Funding

This research was funded by Conselho Nacional de Desenvolvimento Científico e Tecnológico (305819/2017-8), CAPES-Pandemias (88881.504639/2020-01), and Brazilian National Council of Scientific and Technological Development (CNPq) in partnership with Ministry of Science, Technology, Innovations and Communications (MCTIC), and Ministry of Health (MS), Secretariat of Science, Technology, Innovation and Strategic Inputs−Decit/SCTIE 07/2020 (Research to cope with COVID-19, its consequences and other severe acute respiratory syndromes−No. 402432/2020-7).

Notes

The authors declare no competing financial interest.

ACKNOWLEDGMENTS

The authors thank the CAPES (Code 001), UFABC No. 48/2020-REIT (11.01), REVALORES, UFABC, University of São Paulo (USP), Faculty of Medicine of ABC (FMABC), Multiuser Central Facilities (UFABC), Laboratory of Surface Treatment with Plasma (Labplasma), and the researchers Dr. Newton K. Fukushima and Dr. André P. Tschiptschin for the experimental support. This research used facilities of the Brazilian Nanotechnology National Laboratory (LNNano), part of the Brazilian Centre for Research in Energy and Materials (CNPEM), a private nonprofit organization under the supervision of the Brazilian Ministry for Science, Technology, and Innovations (MCTI). The XPS and AFM staffs are acknowledged for their assistance during the experiments (AFM-28009, XPS-20220130, and XPS-20220131 proposals).

REFERENCES

(1) van Doremalen, N.; Bushmaker, T.; Morris, D. H.; Holbrook, M. G.; Gamble, A.; Williamson, B. N.; Tamin, A.; Harcourt, J. L.; Thornburg, N. J.; Gerber, S. I.; Lloyd-Smith, J. O.; de Wit, E.; Munster, V. J. Aerosol and Surface Stability of SARS-CoV-2 as Compared with SARS-CoV-1. *N. Engl. J. Med.* **2020**, *382* (16), 1564−1567.

(2) Asghari, F.; Samiei, M.; Adibkia, K.; Akbarzadeh, A.; Davaran, S. Biodegradable and Biocompatible Polymers for Tissue Engineering Application: A Review. *Artif. Cells, Nanomedicine, Biotechnol.* **2017**, *45* (2), 185−192.

(3) Rebelo, R.; Fernandes, M.; Fangueiro, R. Biopolymers in Medical Implants: A Brief Review. *Procedia Eng.* **2017**, *200*, 236−243.

(4) de Albuquerque, T. L.; Marques Júnior, J. E.; de Queiroz, L. P.; Ricardo, A. D. S.; Rocha, M. V. P. Polylactic Acid Production from Biotechnological Routes: A Review. *Int. J. Biol. Macromol.* **2021**, *186* (July), 933−951.

(5) Hazell, G.; Fisher, L. E.; Murray, W. A.; Nobbs, A. H.; Su, B. Bioinspired Bactericidal Surfaces with Polymer Nanocone Arrays. *J. Colloid Interface Sci.* **2018**, *528*, 389−399.

(6) Ganjian, M.; Modaresifar, K.; Ligeon, M. R. O.; Kunkels, L. B.; Tümer, N.; Angeloni, L.; Hagen, C. W.; Otten, L. G.; Hagedoorn, P.; Apachitei, I.; Fratila-Apachitei, L. E.; Zadpoor, A. A. Nature Helps: Toward Bioinspired Bactericidal Nanopatterns. *Adv. Mater. Interfaces* **2019**, *6* (16), 1900640.

(7) Jeevahan, J.; Chandrasekaran, M.; Britto Joseph, G.; Durairaj, R. B.; Mageshwaran, G. Superhydrophobic Surfaces: A Review on Fundamentals, Applications, and Challenges. *J. Coatings Technol. Res.* **2018**, *15* (2), 231−250.

(8) Ahmad, I.; Kan, C. A Review on Development and Applications of Bio-Inspired Superhydrophobic Textiles. *Materials (Basel).* **2016**, *9* (11), 892.

(9) Müller, F.; Kunz, C.; Gräf, S. Bio-Inspired Functional Surfaces Based on Laser-Induced Periodic Surface Structures. *Materials (Basel).* **2016**, *9* (6), 476.

(10) Palumbo; Lo Porto; Favia. Plasma Nano-Texturing of Polymers for Wettability Control: Why, What and How. *Coatings* **2019**, *9* (10), 640.

(11) Jaggessar, A.; Shahali, H.; Mathew, A.; Yarlagadda, P. K. D. V. Bio-Mimicking Nano and Micro-Structured Surface Fabrication for Antibacterial Properties in Medical Implants. *J. Nanobiotechnology* **2017**, *15* (1), 64.

(12) Fan, X.; Cao, D.; Kong, L.; Zhang, X. Cryo-EM Analysis of the Post-Fusion Structure of the SARS-CoV Spike Glycoprotein. *Nat. Commun.* **2020**, *11* (1), 3618.

(13) Imani, S. M.; Ladouceur, L.; Marshall, T.; Maclachlan, R.; Soleymani, L.; Didar, T. F. Antimicrobial Nanomaterials and Coatings: Current Mechanisms and Future Perspectives to Control the Spread of Viruses Including SARS-CoV-2. *ACS Nano* **2020**, *14* (10), 12341−12369.

(14) Sztajnowski, S.; Krucińska, I.; Sulak, K.; Puchalski, M.; Wrzosek, H.; Bilska, J. Effects of the Artificial Weathering of Biodegradable Spun-Bonded PLA Nonwovens in Respect to Their

Application in Agriculture. *Fibres Text. East. Eur.* **2012**, *96* (6B), 89−95.
(15) Yuniarto, K.; Purwanto, Y. A.; Purwanto, S.; Welt, B. A.; Purwadaria, H. K.; Sunarti, T. C. Infrared and Raman Studies on Polylactide Acid and Polyethylene Glycol-400 Blend. In *AIP Conference Proceedings;* Semarang, Indonesia, 2016; AIP Publishing, 2016; Vol. *1725*, p 020101. DOI: 10.1063/1.4945555.
(16) Harmaen, A. S.; Khalina, A.; Faizal, A. R.; Jawaid, M. Effect of Triacetin on Tensile Properties of Oil Palm Empty Fruit Bunch Fiber-Reinforced Polylactic Acid Composites. *Polym. Plast. Technol. Eng.* **2013**, *52* (4), 400−406.
(17) Luque-Agudo, V.; Hierro-Oliva, M.; Gallardo-Moreno, A. M.; González-Martín, M. L. Effect of Plasma Treatment on the Surface Properties of Polylactic Acid Films. *Polym. Test.* **2021**, *96*, 107097.
(18) Antunes, A.; Luyt, A. S.; Kasak, P.; Aljarod, O.; Hassan, M. K.; Popelka, A. Effect of Plasma Treatment on Accelerated PLA Degradation. *Express Polym. Lett.* **2021**, *15* (8), 725−743.
(19) Coates, J. Interpretation of Infrared Spectra, A Practical Approach. In *Encyclopedia of Analytical Chemistry;* Meyers, R. A., Ed.; John Wiley & Sons, Ltd: Chichester, UK, 2006; pp 10815−10837. DOI: 10.1002/9780470027318.a5606.
(20) Garlotta, D. A Literature Review of Poly(Lactic Acid). *J. Polym. Environ.* **2001**, *9* (2), 63−84.
(21) Lee, H. W.; Insyani, R.; Prasetyo, D.; Prajitno, H.; Sitompul, J. Molecular Weight and Structural Properties of Biodegradable PLA Synthesized with Different Catalysts by Direct Melt Polycondensation. *J. Eng. Technol. Sci.* **2015**, *47* (4), 364−373.
(22) Chamas, A.; Moon, H.; Zheng, J.; Qiu, Y.; Tabassum, T.; Jang, J. H.; Abu-Omar, M.; Scott, S. L.; Suh, S. Degradation Rates of Plastics in the Environment. *ACS Sustain. Chem. Eng.* **2020**, *8* (9), 3494−3511.
(23) Niaounakis, M. *Biopolymers: Applications and Trends;* William Andrew: Oxford, UK, 2015.
(24) Niaounakis, M. *Biopolymers: Reuse, Recycling, and Disposal;* William Andrew: Oxford, UK, 2013.
(25) Sakai, W.; Tsutsumi, N. Photodegradation and Radiation Degradation. In *Poly(Lactic Acid);* Auras, R., Lim, L.-T., Selke, S. E. M., Tsuji, H., Eds.; John Wiley & Sons, Inc.: Hoboken, NJ, 2010; pp 413−421. DOI: 10.1002/9780470649848.ch24.
(26) Koterwa, A.; Kaczmarzyk, I.; Mania, S.; Cieslik, M.; Tylingo, R.; Ossowski, T.; Bogdanowicz, R.; Niedziałkowski, P.; Ryl, J. The Role of Electrolysis and Enzymatic Hydrolysis Treatment in the Enhancement of the Electrochemical Properties of 3D-Printed Carbon Black/Poly(Lactic Acid) Structures. *Appl. Surf. Sci.* **2022**, *574*, 151587.
(27) Renò, F.; D'Angelo, D.; Gottardi, G.; Rizzi, M.; Aragno, D.; Piacenza, G.; Cartasegna, F.; Biasizzo, M.; Trotta, F.; Cannas, M. Atmospheric Pressure Plasma Surface Modification of Poly(D,L-Lactic Acid) Increases Fibroblast, Osteoblast and Keratinocyte Adhesion and Proliferation. *Plasma Process. Polym.* **2012**, *9* (5), 491−502.
(28) Laput, O.; Vasenina, I.; Salvadori, M. C.; Savkin, K.; Zuza, D.; Kurzina, I. Low-Temperature Plasma Treatment of Polylactic Acid and PLA/HA Composite Material. *J. Mater. Sci.* **2019**, *54* (17), 11726−11738.
(29) Qi, Y.; Ma, H.-L.; Du, Z.-H.; Yang, B.; Wu, J.; Wang, R.; Zhang, X.-Q. Hydrophilic and Antibacterial Modification of Poly(Lactic Acid) Films by γ-Ray Irradiation. *ACS Omega* **2019**, *4* (25), 21439−21445.
(30) Siddique, A. B.; Pramanick, A. K.; Chatterjee, S.; Ray, M. Amorphous Carbon Dots and Their Remarkable Ability to Detect 2,4,6-Trinitrophenol. *Sci. Rep.* **2018**, *8* (1), 1−10.
(31) da Silva, D. J.; da Silva Barbosa, R. F.; de Souza, A. G.; Ferreira, R. R.; Camani, P. H.; Nantes-Cardoso, I. L.; Rosa, D. S. Bactericidal Activity of Cotton Fabrics Functionalized by ZnO and Cu via Microwave. *Cellulose* **2021**, *28* (12), 8153−8175.
(32) Rebhan, B.; Tollabimazraehno, S.; Hesser, G.; Dragoi, V. Analytical Methods Used for Low Temperature Cu-Cu Wafer Bonding Process Evaluation. *Microsyst. Technol.* **2015**, *21* (5), 1003−1013.
(33) Bui, N. T.; Kang, H.; Teat, S. J.; Su, G. M.; Pao, C.-W.; Liu, Y.-S.; Zaia, E. W.; Guo, J.; Chen, J.-L.; Meihaus, K. R.; Dun, C.; Mattox, T. M.; Long, J. R.; Fiske, P.; Kostecki, R.; Urban, J. J. A Nature-Inspired Hydrogen-Bonded Supramolecular Complex for Selective Copper Ion Removal from Water. *Nat. Commun.* **2020**, *11* (1), 3947.
(34) Phan, L.; Yoon, S.; Moon, M.-W. Plasma-Based Nanostructuring of Polymers: A Review. *Polymers (Basel).* **2017**, *9* (12), 417.
(35) Žigon, J.; Karič, M.; Pavlič, M. Surface Finishing of 3d-Printed Polymers with Selected Coatings. *Polymers (Basel).* **2020**, *12* (12), 1−14.
(36) Popelka, A.; Abdulkareem, A.; Mahmoud, A. A.; Nassr, M. G.; Al-Ruweidi, M. K. A. A.; Mohamoud, K. J.; Hussein, M. K.; Lehocky, M.; Vesela, D.; Humpolíček, P.; Kasak, P. Antimicrobial Modification of PLA Scaffolds with Ascorbic and Fumaric Acids via Plasma Treatment. *Surf. Coat. Technol.* **2020**, *400* (July), 126216.
(37) Izdebska-Podsiadły, J.; Dörsam, E. Effects of Argon Low Temperature Plasma on PLA Film Surface and Aging Behaviors. *Vacuum* **2017**, *145*, 278−284.
(38) Shah, M.; Woo, H. G. Omicron: A Heavily Mutated SARS-CoV-2 Variant Exhibits Stronger Binding to ACE2 and Potently Escapes Approved COVID-19 Therapeutic Antibodies. *Front. Immunol.* **2022**, *12*, 1−10.
(39) Cervantes-Cervantes, M. P.; Calderón-Salinas, J. V.; Albores, A.; Muñoz-Sánchez, J. L. Copper Increases the Damage to DNA and Proteins Caused by Reactive Oxygen Species. *Biol. Trace Elem. Res.* **2005**, *103* (3), 229−248.
(40) Angele-Martinez, C.; Nguyen, K. V. T.; Ameer, F. S.; Anker, J. N.; Brumaghim, J. L. Reactive Oxygen Species Generation by Copper(II) Oxide Nanoparticles Determined by DNA Damage Assays and EPR Spectroscopy. *Nanotoxicology* **2017**, *11* (2), 278−288.
(41) Liu, J.; Wang, J.; Lee, S.; Wen, R. Copper-Caused Oxidative Stress Triggers the Activation of Antioxidant Enzymes via ZmMPK3 in Maize Leaves. *PLoS One* **2018**, *13* (9), e0203612.
(42) Vodnar, D. C.; Mitrea, L.; Călinoiu, L. F.; Szabo, K.; Ştefănescu, B. E. Removal of Bacteria, Viruses, and Other Microbial Entities by Means of Nanoparticles. In *Advanced Nanostructures for Environmental Health;* Elsevier, 2020; pp 465−491. DOI: 10.1016/B978-0-12-815882-1.00011-2.
(43) da Silva, D. J.; Souza, A. G.; Ferreira, G. da S.; Duran, A.; Cabral, A. D.; Fonseca, F. L. A.; Bueno, R. F.; Rosa, D. S. Cotton Fabrics Decorated with Antimicrobial Ag-Coated TiO2 Nanoparticles Are Unable to Fully and Rapidly Eradicate SARS-CoV-2. *ACS Appl. Nano Mater.* **2021**, *4* (12), 12949−12956.
(44) Meister, T. L.; Fortmann, J.; Breisch, M.; Sengstock, C.; Steinmann, E.; Köller, M.; Pfaender, S.; Ludwig, A. Nanoscale Copper and Silver Thin Film Systems Display Differences in Antiviral and Antibacterial Properties. *Sci. Rep.* **2022**, *12* (1), 7193.